Progress in Materials Chemistry and Physics (2022)
Clausius Scientific Press, Canada

DOI: 10.23977/pmcp.2022.030102
ISSN 2616-3780 Vol. 3 Num. 1

Study on the Mechanism of the Generation of Plaque Defects on the Tooth Surface of High Speed Railway Transmission Gears

Hui Li*

Hydrogen Link (Jiangsu) High Tech Co., Ltd., Changzhou, 213164, China
**Corresponding author*

Keywords: Transmission gears, Galvanic corrosion, Friction, Wear

Abstract: High-speed railways play an important role in the development of the national regional economy, where the performance of the transmission gears directly affects their reliability and safety. A study was conducted to investigate the mechanism of the defect through chemical composition inspection, macroscopic observation, microscopic morphology, hardness testing and microstructure analysis of a regular crater defect on the tooth surface of a transmission gear found in the maintenance of a high-speed railway train. The results of the study show that the crater defect is a partial melt and mechanical wear caused by galvanic corrosion, which is due to inadequate insulation of the rail to ground and partial dispersion of the current breaking through the thin oil film between the high-speed rotating gears to produce spark discharge, which in turn forms galvanic corrosion.

1. Introduction

High-speed rail is an important infrastructure that drives the national economy to take off, and plays an increasingly important role in the process of national regional economic development [1-2]. The gear transmission system is the core component of the energy conversion and transmission of high-speed trains, and its working performance directly affects the reliability and safety of the operation of high-speed trains, and is also the key to the "world speed" of China's high-speed trains [3-4].

The gearing system consists of gears, boxes, bearings and lubrication mechanisms, and is the core component that allows trains to travel at high speeds [5-6]. Generally speaking, a gearbox with a linear speed of more than 25 metres per second can be called a high-speed gearbox, and at 380 kilometres per hour, the linear speed of the driven gears needs to reach 70 metres per second [7-8]. Such a high speed poses a great challenge to the performance of the gear itself, the meshing between the gears and the reliability of the sealing of the box [0-0]. A train was overhauled after 600,000 km of operation and multiple pit defects were found in the root area of the large gear and the top area of the pinion.

In this paper, the pitted defective transmission gear was analysed by chemical composition inspection, macroscopic observation, microscopic morphology, hardness testing and microstructure analysis to determine the mechanism by which the transmission gear defect was produced and to

qualitatively analyse the causes of its production, with a view to providing analytical methods and references to avoid the recurrence of such incidents.

2. Physical and Chemical Testing

2.1. Chemical Composition Test Results

The active pinion gear material in this gear transmission system is 20CrNiMo alloy structural steel, the implementation standard GB/T 3077-1999, heat treatment process is normalized + carburizing + quenching, hardening layer depth 1.2-1.7mm, tooth surface hardness 650-780HV; driven large gear material is S40C alloy, the implementation standard JIS G1054-2005, heat treatment process Quenching + induction quenching, tooth surface hardness 500-700HV, tooth root hardness above 200HV. In accordance with GB/T 20123-2006, CS901B infrared carbon and sulphur meter was used to determine the content of sulphur and phosphorus; in accordance with GB/T 4336-2016, ARL4460 photoelectric direct reading spectrometer was used to determine the content of other elements, and the results are shown in Table 1. It can be seen that the chemical composition of the large and small gear substrate are in line with the technical requirements of the relevant material specifications.

Table 1: Gear chemical composition test results (mass, %)

Ingredient	C	Si	Mn	P	S	Cr	Ni	Mo	Cu
Pinion	0.21	0.27	0.53	0.017	0.002	0.5	1.7	0.26	0.1
20CrNiMo [16]	0.17~0.23	0.20~0.35	0.40~0.70	≤0.030	≤0.030	0.35~0.65	1.60~2.00	0.20~0.30	≤0.30
Large gears	0.4	0.18	0.77	0.018	0.017	0.16	0.02	0.01	0.01
S40C steel [17]	0.37~0.43	0.15~0.35	0.60~0.90	≤0.030	≤0.035	≤0.20	≤0.20	/	≤0.30

2.2. Macro View

The gear set was disassembled and cleaned, and its macroscopic shape is shown in Figure 1. As can be seen from the figure, the defect on the large gear (driven wheel) is located near the root of the tooth, with a patchy melt feature and a tempering colour, and the surface of the tooth around the defect is intact. The defect on the pinion (active wheel) is located near the top of the tooth, basically distributed on the same circumference, the defective surface has obvious tempering characteristics, local blue or light yellow, the internal is a dotted pit loaded molten state, local appearing spot type wear area, the area and the large gear tooth surface spot position corresponds exactly, the defect around the tooth surface grinding traces are clearly visible, no obvious abnormalities, non-defective area tooth surface is intact no bias load bias grinding phenomenon was found [12-13].

(**a**) (**b**) (**c**)

(a) Defective large gear (driven wheel); (b) Pinion (main wheel) defects; (c) Crater defects enlarged.

Figure 1: Macroscopic appearance of gear tooth crater defects

2.3. Low Magnification Erosion Morphology and Hardness Inspection

The tooth surface was cut vertically along the defective large gear and pinion teeth respectively

and the sections were made into low magnification specimens [14-18]. Figure 2 shows a low-frequency photo of the erosion by ethanol nitrate solution. The low-frequency erosion shows that the hardened layer of the pinion is uniformly distributed and has the characteristics of carburising quenching; the hardened layer of the large gear is thicker at the top of the tooth and shallower at the root of the tooth and has the characteristics of induction quenching. No abnormalities such as burns were observed on the tooth surfaces of both the large and small gears.

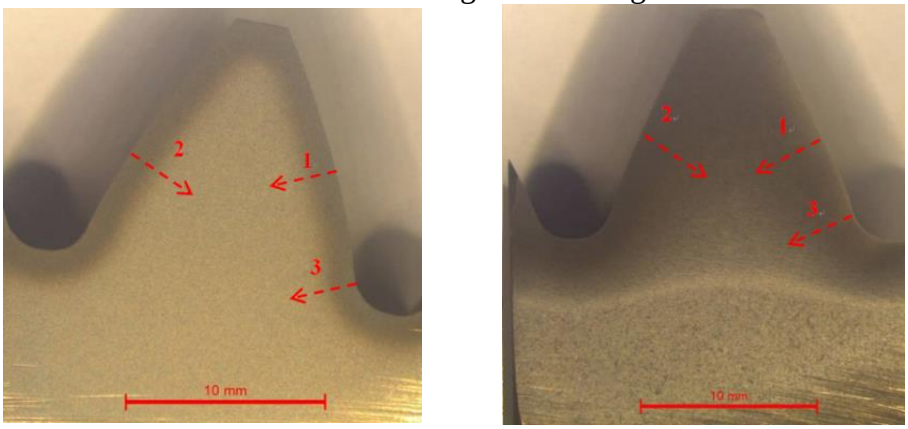

(a) (b)

(a) Pinion (main wheel); (b) Large gear (driven wheel).

Figure 2: Low magnification photograph of the defective section of the gear

Separate samples of large and small gear defects and their nearby areas, using FM-700 Vickers hardness tester hardness test, each to three test points, the results are shown in Table 2, can be seen at the defective hardness and the nearby area difference is small, no obvious hardness drop.

Table 2: Microhardness test results at gear defects (HV0.1)

Test area	Active gear tooth top defect	Active gear tooth face	Slave gear tooth roots with spotted defects	Slave gear tooth surface line defect	Slave gear tooth surface
Microhardness	717, 710, 728	712, 720, 718	590, 587, 583	592, 587, 580	587, 580, 583

The hardness gradient test was carried out at 1, 2 and 3 in Figure 2, and the hardness test curve is shown in Figure 3, which shows that the depth of the carburizing layer of the pinion is: CHD513HV1.0:1.810mm on one side of the pitch circle; CHD513HV1.0:1.798mm on the other side of the pitch circle; and CHD513HV1.0:1.504mm at the root of the tooth. DS435HV1.0:2.845mm on one side; DS435HV1.0:2.830mm on the other side of the pitch circle; DS435HV1.0:1.410mm on the root of the tooth.

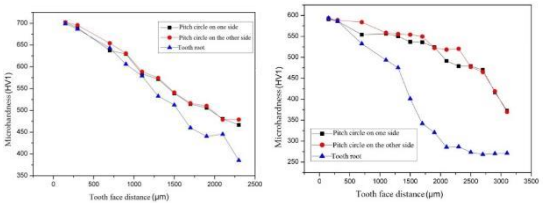

(a) (b)

(a) Pinion (main wheel); (b) Large gear (driven wheel).

Figure 3: Microhardness gradient curves for large and small gears

2.4. Microform

The pinion tooth surface defects at the line cutting system sample, after ethanol ultrasonic cleaning, using Hitachi S-3700N scanning electron microscope to observe the tooth surface crater defects, microscopic morphology as shown in Figure 4. From the overall morphology of the defect, it can be seen that there are puffy cloud-like round spots in the defective depressions, with local presence of fine round beads and a rounded surface with free solidification surface characteristics. Tooth surface defects and normal tooth surface at the junction of the micro-existence of small beads and parallel distribution of tooth surface grinding traces, with galvanic corrosion "molten beads" morphological characteristics.

Galvanic corrosion is due to the action of electric arcs or sparks radiating between the gear meshing tooth surfaces, the formation of many small arc pits with smooth edges on the gear tooth surface, with molten discharge characteristics, the tooth surface will sometimes also appear a large area of burns, the edge of which shows a tempered colour [19-20]. The presence of molten beads indicates that the area was subjected to very high temperatures in service, resulting in localised melting. The high temperatures may be related to the transient high pressures of the HRL lines, where the instantaneous high pressures lead to local spark discharges when the gears are engaged or separated, causing the local temperature to rise sharply and exceed the melting point of the metal, resulting in the formation of molten beads on the tooth surface, also known as galvanic erosion [21-22].

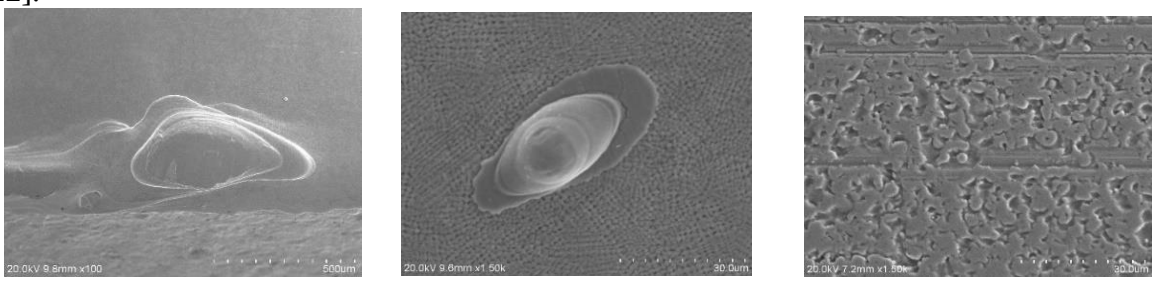

(a) (b) (c)

(a) Overall shape; (b) Floating cloud-like spots; (c) Small fused beads.

Figure 4: Microscopic appearance of pinion defects

The same method was used for the scanning electron microscope morphology test of the large gear defect, as shown in Figure 5, the defect depression there are floating clouds of round spots, with free solidification surface characteristics, and melt droplets local sputtering. Most of the defect area is polished, the defect at the root of the tooth has obvious plastic extension deformation, a small part has been extended to the root of the tooth unground area, the area against the tooth surface can be seen a large number of craters, the bottom of the crater is relatively smooth, showing a cloud-shaped pattern, has the characteristics of fatigue wear (or contact fatigue). This is due to the fatigue damage that occurs locally when the oil film cannot be established at the defective area during the subsequent operation after galvanic corrosion has occurred on the meshing tooth surface.

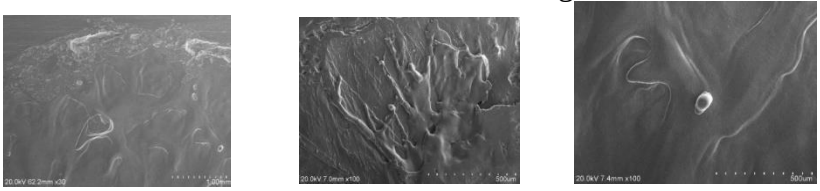

(a) (b) (c)

(a) Overall morphology; (b) Sputtering droplets; (c) Floating cloud-like spots.

Figure 5: Microscopic appearance of large gear defects

The results of the energy spectroscopy tests carried out on the defective tooth face, shown in Figure 6, show that the area is dominated by the base elements of the gear steel and no slag defects are characteristic.

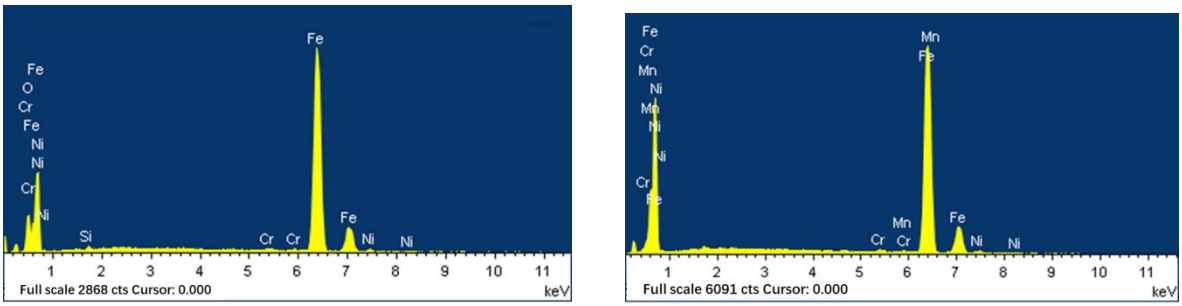

(a) (b)

(a) Pinion gear; (b) Large gear.

Figure 6: Results of energy spectrum analysis area at tooth surface defects

2.5. Microstructure

From the large and small gears on the spot area and away from the spot on the normal substrate were cut metallographic specimens, after inlay, grinding and polishing in 4% v/v) nitric acid alcohol solution corrosion, in LEICADMI5000M type optical microscope to observe the microstructure [23-24]. Active gear metallographic organization as shown in Figure 7, by the figure can be seen: active pinion normal regional cross-sectional metallographic organization, pitch round surface layer metallographic organization for needle martensite + about 5% residual austenite + diffuse granular carbide. The surface layer of the tooth root is needle martensite + approximately 5% residual austenite + diffuse granular carbide. The core of the tooth block is bainite + slate-like martensite + ferrite, which is typical of carburising and quenching [25], with no abnormalities in the heat treatment process.

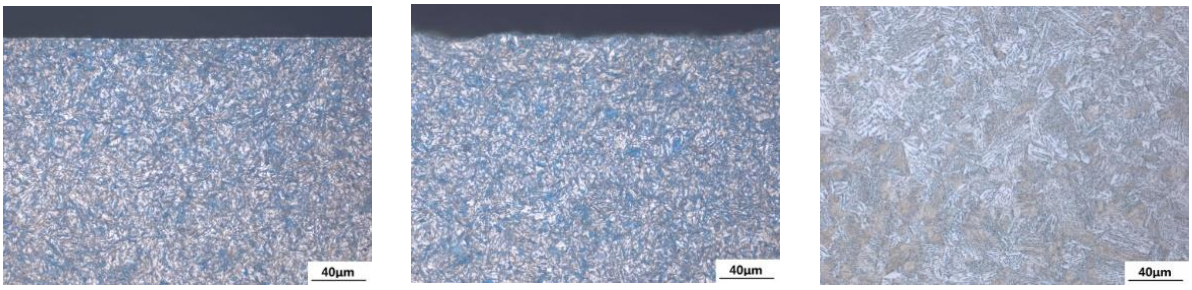

(a) (b) (c)

(a) Surface layer of pitch circle; (b) Surface layer of tooth root; (c) Core of tooth block.

Figure 7: Metallographic organization of the active gear

The surface layer of the pitch circle of the driven large gear and the core of the tooth block are similar to those of the active gear, and no abnormalities are seen in the heat treatment process. The surface layer of the tooth root has a non-martensite layer about 21μm deep, and the sub-surface layer is needle martensite + about 3% residual austenite + diffuse granular carbide, as shown in Figure 8(a). The metallographic organisation of the section at the defect is shown in Figure 8(b), where there is a white bright layer on the surface, a black tempered layer on the sub-surface and a yellow-brown carburised quenched layer on the interior, indicating that the area had experienced higher temperatures and localised micro-cracking sprouting, with shallow crack depths limited to the quenched martensite range.

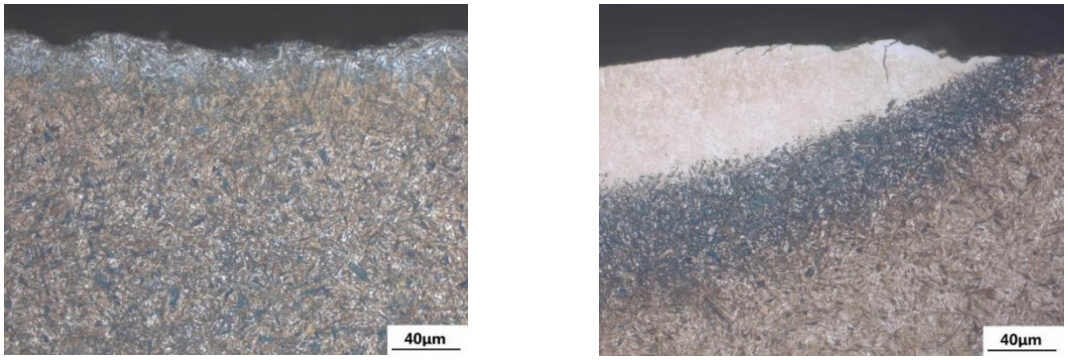

(a) (b)

(a) Surface layer of tooth root; (b) Defective interface.

Figure 8: Metallographic organization of driven gear

3. Results and Discussion

From the physical and chemical inspection results, it can be seen that: the chemical composition of the large and small gears meets the requirements; the carburizing characteristics of the teeth of the small gears exist, and the surface hardness and depth of the carburizing layer meet the technical requirements; the teeth of the large gears have been surface hardened, and the surface hardness meets the technical requirements, and the microstructure is not abnormal, and there are micro cracks in the area of the speckles; the speckles on the large gears are located at the root of the teeth, and the speckles on the small gears are located at the top of the teeth. The shape, size and position of the different scars on the large and small gears are the same; the gears are not well meshed and there is a good correspondence between the position of the scars and the state of the gears when they are meshed; the presence of a large number of molten beads in the area of the scars on the small gears indicates that the gears were subjected to high temperatures in service, resulting in localised melting, and some of the molten beads have a flattened shape, indicating that the molten beads were subjected to extrusion and wear when the gears were meshed.

Under normal circumstances, there is a thin film of oil between the teeth of the gears that mesh with each other during operation, and the lubricant can also play a certain role in cooling the teeth so that the temperature of the teeth does not rise too high. However, when the insulation of the train circuit is poor and the insulation of the tracks to ground is inadequate, some stray currents will flow through the high speed rotating gears, penetrating the thin oil film between the teeth and generating spark discharges, leading to galvanic corrosion; to a lesser extent this will lead to carbonisation of the oil film, to a greater extent it will lead to localised melting of the gear contact parts to form molten beads, which will become uneven, thus forming a patch. The rapid absorption of heat during the formation of the bead causes a rapid drop in temperature, resulting in a secondary quench, which may cause quench micro-cracks. In addition, this area may also crack under the squeezing action of continued meshing. At the same time, the molten beads in the discharge area take on a flattened shape due to the squeezing and abrasive action during gear engagement.

The presence of galvanic corrosion is not the only cause of rapid gear failure. Likewise, tooth surface failure is not exclusively caused by frictional wear. Rapid gear failure is often the result of an alternating combination of the two. The molten metal in the molten state after the galvanic discharge forms a white bright layer under the action of the lubricating fluid cooling, the white bright layer is quenched martensite, high hardness, brittleness, in the frictional wear process is very easy to sprout microscopic cracks and expansion, making the local metal off, forming craters. In addition, the raised part of the electro-etching pit area produces metal particles in the repeated meshing, both of which are

mixed in the lubricating oil to form an abrasive, deteriorating the lubricating environment and thus aggravating the gear wear leading to its early failure.

4. Conclusions and Countermeasures

The gear set was subjected to galvanic friction wear, due to poor insulation of the train circuit and inadequate insulation of the tracks to ground, part of the stray current penetrated the thin oil film between the tooth surfaces and generated spark discharge, resulting in galvanic corrosion; the crater-like defects on both the large and small gears were characterised by a molten state, the microstructure was a high hard, high brittle quenched martensite, which was highly susceptible to microscopic cracking and expansion, coupled with galvanic corrosion making it impossible to establish a local oil film, resulting in wear of the gears under cyclic meshing and contact fatigue spalling, resulting in crater-like defects.

Based on the above conclusions, the following aspects can be addressed: improve the grinding accuracy of the gear tooth surface to avoid the appearance of obvious grinding tool marks; ensure adequate lubrication between the meshing surfaces of the master and driven gears and carry out regular checks on the oil quality in the gearbox to prevent deterioration of the oil quality; strengthen the insulation control to the ground after the rail is laid to ensure that the leakage current is within the technical requirements and adopt a reasonable grounding device.

References

[1] Mejuto Diego, G. (2022) Theorizing nation-building through high-speed rail development: Hegemony and space in the Basque Country, Spain. Environment and Planning A: Economy and Space, 54, 554-571.

[2] Ruobing, K.; Zhigang, K. (2021) Structural Strength Analysis of High Current Connector for Rail Transit. Journal of Physics: Conference Series, 2095, 012-023.

[3] Xin, L.; Yu, Y.; Zhantao, W.; Ke, Y.; Haidong, S.; Junsheng, C. (2022) High-accuracy gearbox health state recognition based on graph sparse random vector functional link network. Reliability Engineering and System Safety, 218, 108-117.

[4] Feng, Y.; Xiaochun, Z.; Chunyu, L.; Jun, L. (2021) Analysis and Research on Fracture Cause of Fixed Shaft of Torsion Arm of Wind Turbine Gearbox. Journal of Physics: Conference Series, 2133, 012-039.

[5] Yunmin, W.; Guohua, C.; Youliang, Y.; Jingjing, W. (2022) Does high-speed rail stimulate cross-city technological innovation collaboration? Evidence from China. Transport Policy, 116, 119-131.

[6] Gronostajski, Z.; Hawryluk, M.; Widomski, P.; Kaszuba, M.; Nowak, B.; Polak, S.; Rychlik, M.; Ziemba, J.; Zwierzchowski, M. (2019) Selected effective methods of increasing the durability of forging tools in hot forging processes. Procedia. Manuf, 27, 124–129.

[7] Yanliang,N.; Huimin, L.; Kunhui, Y.; Amin,M.; Xiaopeng, D. (2022) Determinants of Coopetition Relationships in International Joint Ventures for High-Speed Rail Projects. KSCE Journal of Civil Engineering, 04, 1-22.

[8] Ke Liang, W.; Su Qin, P.; Fu Qin, Z.; Zhuang, M. (2022) Does high-speed rail improve China's urban environmental efficiency? Empirical evidence from a quasi-natural experiment. Environmental Science and Pollution Research 11, 1-22.

[9] Zhenhua, C.; Anthony, P.;Xingju, W. (2021)High-speed rail and the environment. Transportation Research Part D, 101, 103-112.

[10] Yahong, L.; Chengxiang, T.;Tao, B.; Daisheng, T. (2021) Association of High-Speed Rail and Tuberculosis Transmission in Newly Integrated Regions: Quasi-Experimental Evidence from China. International Journal of Public Health, 66, 160-169.

[11] Shengli, C.; Shaowen, W.; Caijun, Z.; Qingjun, Z. (2022) Three-Dimensional Morphology and Analysis of Widmanstätten Sideplates Ferrite. Metals, 12, 523-530.

[12] JinSeok, P.; JeongHyeon, K.; YongCheol, J.; HeeTae, K.; SeulKee, K.; JaeMyung, L. (2022) Effect of Corrugated Sheet Diameter on Structural Behavior under Cryogenic Temperature and Hydrodynamic Load. Metals, 12, 521-531.

[13] Jon,S.; Jacques, L. (2022)Casting Defects in Sand-Mold Cast Irons—An Illustrated Review with Emphasis on Spheroidal Graphite Cast Irons. Metals, 12, 504-516.

[14] Chunsheng, C.; Jinhao, N.; Yuxin, L.; Qingfeng, G.; Jie, C.; Pengfei, Z.; Jie, W. (2022) Wear Resistance of FeCrAlNbNi Alloyed Zone via Laser Surface Alloying on 304 Stainless Steel. Metals, 12, 467-478.

[15] Uchic, M.D.; Groeber, M.A.; Dimiduk, D.M.; Simmons, J.P. (2006) 3D micro structural characterization of nickel superalloys via serial-sectioning using a dual beam FIB-SEM. Scr. Mater, 55, 23–28.
[16] Cao, S.; Tirry, W.; Van Broek, D.; Schryvers, D. (2009) Optimization of a FIB/SEM slice-and-view study of the 3D distribution of Ni4Ti3 precipitates in Ni–Ti. J. Microsc, 233, 61–68.
[17] Zankel, A.; Wagner, J.; Peter, P. (2014) Serial sectioning methods for 3D investigations in materials science. Micron, 62, 66–78.
[18] Thiago, D.; Yuri A., M.; Wislei R, O. (2022) The Holes of Zn Phosphate and Hot Dip Galvanizing on Electrochemical Behaviors of Multi-Coatings on Steel Substrates. Metals, 12, 863-872.
[19] QiWei, W.; JunXi, Z.; Yan,G.; NianWei, D.; YunXiang, C.; DeYuan, L.; XiaoJian, X. (2022)Galvanic Effect and Alternating Current Corrosion of Steel in Acidic Red Soil. Metals, 12, 296-305.
[20] Pei, Z.; Xiao, K.; Lihong, C.; Qing, L.; Jun, W.; Lingwei, M.; Xiaogang, L. (2020) Investigation of Corrosion Behaviors on an Fe/Cu-Type ACM Sensor under Various Environments. Metals, 10, 905-912.
[21] Kangchun, L.; Seho, S.; Ganggyu, L.; Gyeonghui, Y.; Donghyeok, K.; Junha, H.;Hojin, J.; Taeseup, S.; Ungyu, P. (2021)Galvanic corrosion inhibition from aspect of bonding orbital theory in Cu/Ru barrier CMP. Scientific Reports, 11, 212-224.
[22] Groeber, M.A.; Haley, B.K.; Uchic, M.D. (2006)3D reconstruction and characterization of polycrystalline microstructures using a FIB-SEM system. Mater. Charact, 57, 259–273.
[23] Fan, G.H.; Zhang, Y.B.; Driver, J.H.; Jensen, D.J. (2014) Oriented growth during recrystallization revisited in three dimensions. Scr. Mater, 72, 9–12.
[24] Wu, S.; Zhang, C.; Zhu, L.; Zhang, Q.; Ma, X. (2020) In-depth analysis of intragranular acicular ferrite three-dimensional morphology. Scr. Mater, 185, 61–65.
[25] Finn, S.; Franziska, R.; Sören, E.; Carey Leroy, W.; Moritz, B. (2022) Relation between the Fatigue and Fracture Ductile-Brittle Transition in S500 Welded Steel Joints. Metals, 12, 385-396.